

Article

A Multifunctional Isolated and Non-Isolated Dual Mode Converter for Renewable Energy Conversion Applications

Yiwan Wang ^{1,2,*}, Chun Gan ³, Kai Ni ⁴ , Xinhua Li ⁴, Houjun Tang ¹ and Yong Yang ⁵

¹ Department of Electrical Engineering, Shanghai Jiao Tong University, Shanghai 200240, China; hjtang@sjtu.edu.cn

² School of Electronic and Information Engineering, Suzhou Vocational University, Suzhou 215104, China

³ Department of Electrical Engineering and Computer Science, University of Tennessee, Knoxville, TN 37996, USA; cgan@utk.edu

⁴ Department of Electrical Engineering and Electronics, University of Liverpool, Liverpool L69 3GJ, UK; k.ni@student.liverpool.ac.uk (K.N.); xinhua.li@liverpool.ac.uk (X.L.)

⁵ School of Urban Rail Transportation, Soochow University, Suzhou 215137, China; yangy1981@suda.edu.cn

* Correspondence: wyiwan@163.com; Tel.: +86-158-5018-3606

Received: 16 October 2017; Accepted: 25 November 2017; Published: 30 November 2017

Abstract: In this paper, a multifunctional isolated and non-isolated dual-mode low-power converter was designed for renewable energy conversion applications such as photovoltaic power generation to achieve different operating modes under bi-directional electrical conversion. The proposed topology consists of a bidirectional non-isolated DC/DC circuit and an isolated converter with a high-frequency transformer, which merge the advantages of both the conventional isolated converter and non-isolated converter with the combination of the two converter technologies. Compared with traditional converters, the multifunctional converter can not only realize conventional bi-directional functions, but can also be applied for many different operation modes and meet the high output/input ratio demands with the two converter circuits operating together. A novel control algorithm was proposed to achieve the various functions of the proposed converter. An experimental platform based on the proposed circuit was established. Both the simulation and experimental results indicated that the proposed converter could provide isolated and non-isolated modes in different applications, which could meet different practical engineering requirements.

Keywords: multifunctional converter; bi-directional; isolated and non-isolated; dual mode; control

1. Introduction

With the development of power electronics, solid state converters have been widely used in several renewable energy applications [1–6]. Different applications require different converter topologies, which can be divided into isolated and non-isolated converters. In recent years, with further renewable energy systems, new requirements for power electronic conversion have been proposed.

Currently, there are some converter topologies for solar power and other renewable energy applications [6–9]. Generally, the grid-connected systems use non-isolated converters in most conditions. In some distributed power generators, a single-phase two-stage transformerless circuit is usually used, and the converter can be used to step up the DC voltage [10] in the similar way to boost and buck-boost converters [11]. These topologies are suitable for grid-connected applications with high efficiency, low cost, and compact structures [12,13]. However, in stand-alone system applications, isolated converters or inverters are mostly employed in the power conversion circuits [14–19].

In [20], a power system using a high step-up converter for dc load applications in a photovoltaic energy conversion system was presented. The developed converter adopted a coupled inductor

and a boost converter working in interleaved mode. A novel high step-up DC-DC converter was successfully integrated using a coupled inductor and the switched capacitor techniques described in [21]. Nevertheless, these converters only control the power flow from the input array to loads in a unique direction or could not achieve galvanic isolation applications. With the emergence of new energy applications, compared with the single-function of a grid-connected or off-grid (stand-alone) system, new dual-mode [22,23] or multifunctional applications [24,25] have become more popular, which are a new trend in the future for renewable energy applications [19]. As different conversion modes are required in different applications, more flexible and reliable conversion circuits are needed. This paper proposes a new multifunctional isolated and non-isolated dual mode low-power converter, and shows a block diagram of the proposed converter system is shown in Figure 1.

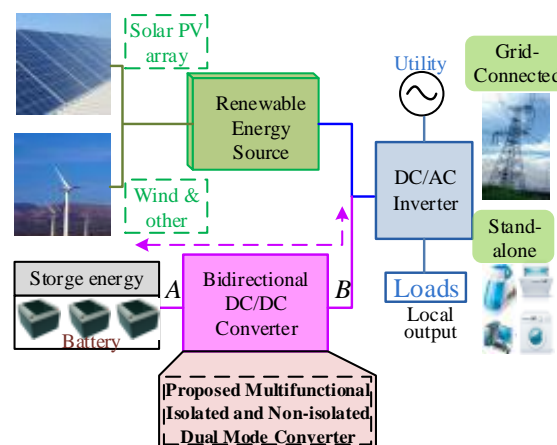


Figure 1. Block diagram of the proposed converter application system.

Compared to traditional converters, with the addition of the realization of conventional bi-directional function, the multifunctional converter can also be applied for both the isolated and non-isolated operation modes. Switching between the isolated and non-isolated operation modes is presented according to different applications by adjusting the control switch signals, which are flexible to change in the operation mode for renewable energy conversion applications. The simulation and experimental results indicated that the proposed topology could provide an efficient isolated or non-isolated dual mode converter under different applications and meet the different practical engineering requirements.

The paper is organized as follows: Section 2 describes the topology of the proposed multifunctional converter. Different operation modes and control strategies are explained in Section 3. Section 4 introduces the design of key parameters for the proposed converter. In Section 5, the simulation tests and experimental results are displayed and discussed. Finally, the conclusions are presented in Section 6.

2. Proposed Multifunctional Isolated and Non-Isolated Dual Mode Converter

The single bidirectional buck/boost non-isolated converter or flyback isolated converter is a DC/DC electrical power conversion solution for grid-connected or stand-alone energy system projects due to their technical maturity. The flyback converter has been widely used in a large number of power conversions due to its relatively simple structure, good performance, and galvanic isolation [26–28]. A bidirectional buck/boost converter is a mature topology in power electronics systems due to its simplicity and high efficiency [29]; however, the conventional buck/boost converter cannot achieve input and output galvanic isolation. To simultaneously implement the functions of isolated and non-isolated converters and benefit from the advantages of the two converter circuits, this paper proposes a novel multifunctional isolated and non-isolated dual mode converter by increasing the

control transfer units. The design methodology of the proposed new converter is depicted in Figure 2. Since the conventional bidirectional buck/boost converter and flyback converters are complementary in galvanic and other technical characteristics, it is feasible and reasonable to combine them to create a new multifunctional isolated/non-isolated dual mode converter where the buck/boost converter operates in the non-isolated operation mode and the flyback converter operates in the isolated operation mode. The new converter contains a non-isolated bidirectional step-up and step-down front-stage circuit, an isolated converter, and a conversion control switching circuit. By adjusting the controllable devices and transfer switches, the different operation modes can be interchanged.

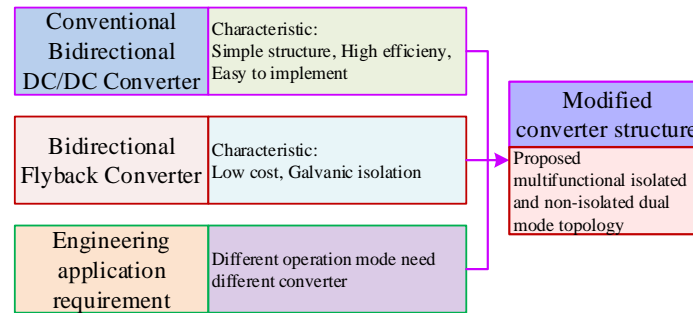


Figure 2. The design methodology of proposed new converter.

The schematic of the proposed converter is illustrated in Figure 2. It consists of a bidirectional non-isolated conventional DC/DC circuit and an isolated converter with a high-frequency transformer, and these two parts are connected by the transfer switches. A common buck/boost bi-directional converter is employed as the non-isolated stage converter including a conventional non-isolated bidirectional step-up and step-down circuit in the proposed topology. The isolated stage converter is composed of a bidirectional flyback converter.

The proposed circuit schematic is shown in Figure 3, where U_1 and U_2 denote the port1 (DC bus or U_1 side) voltage and the port2 (storage system or U_2 side) voltage, respectively. S_1 (D_1), S_2 (D_2), S_{i1} (D_{i1}), and S_{i2} (D_{i2}) are fully-controlled power electronic switching devices in the converter; S_{i1} and S_{i2} are the switches in the isolated converter; C_1 and C_2 are the non-isolated converter capacitors; C_3 represents the filter capacitor; L is the inductor of a non-isolated converter; and T is the isolated stage converter flyback transformer.

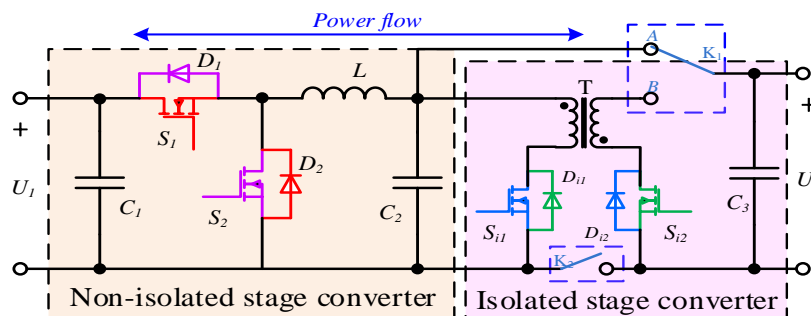


Figure 3. Proposed multifunctional bidirectional dual-mode converter.

The proposed new dual-mode converter merges the advantages of both the conventional isolated converter and non-isolated converter to create a blend of two types of converter technologies. The new converter not only copes with the common function requirements, but also meets the high output/input ratio demands when the two converter circuits operate together.

As previously depicted, the proposed new converter topology is an integrated conventional bidirectional buck/boost circuit and a bidirectional flyback circuit. The novel converter works in two different modes.

2.1. Isolated Mode

In this mode, the bidirectional flyback converter is working. The equivalent circuit of the isolated operating mode is shown in Figure 4. In this operation mode, the trigger switch relay K_1 is switched to contact node B, and the switch relay K_2 is closed.

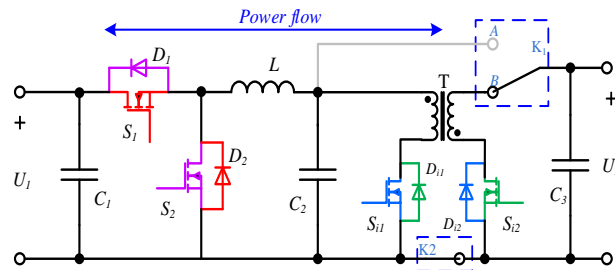


Figure 4. The equivalent circuits of the proposed converter in isolated operation.

There are three working states in this operation mode, including the forward conversion state, reverse conversion state, and the fault protection state. In the forward conversion state, the proposed converter transfers the power from the U_2 -side to the U_1 -side. Since the converter works as a storage system discharge, this state is called the discharge mode.

The equivalent circuit of the forward conversion state is presented in Figure 5a. The switch S_{12} operates in the Pulse Width Modulation (PWM) mode, and the power flow through the flyback and the equivalent boost converter into the output loads. In this state, when the system requires a high conversion ratio, the converter can operate in the combination conversion state, which means that S_2 is controlled by a high frequency PWM signal, otherwise S_2 is turned off.

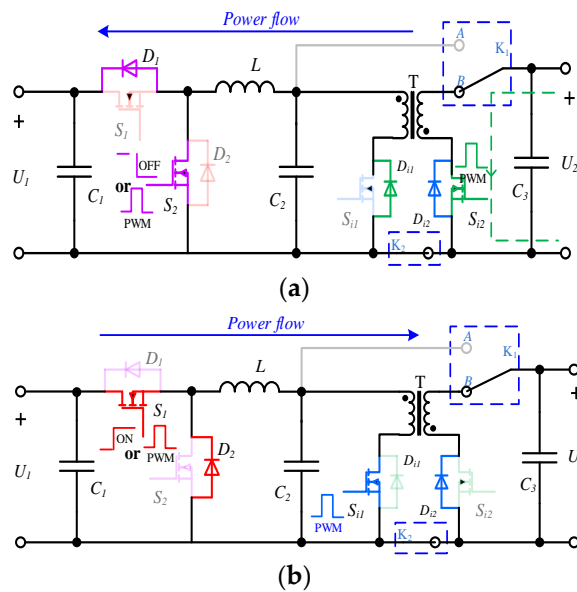


Figure 5. Cont.

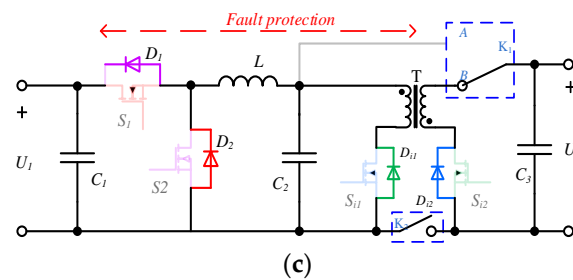


Figure 5. Three operating states of the isolated mode: (a) forward conversion stage; (b) reverse conversion stage; and (c) fault protection stage.

The equivalent circuit of the reverse conversion state is shown in Figure 5b. The operation control is similar to that in the forward conversion state, while the difference is in the direction of power flow. When switch S_{i1} operates in the PWM mode, the topology is an equivalent circuit of a buck converter (high conversion ratio when PWM duty cycle is less than one $DSiPWM < 1$) or filter circuit (when the PWM duty cycle is equal to one $DSiPWM = 1$) with the flyback converter charging the storage system from the U_1 -side (such as the DC bus).

As displayed in Figure 5c, if any external fault occurs in the system, the converter enters the fault-protection stage. To achieve electrical isolation between the critical equipment and components, all PWM control signals are turned off at this stage, then the fully-controlled switches $S_1 \setminus S_2 \setminus S_{i1}$ and S_{i2} are turned off. The trigger switch K_1 is switched onto contact B and switch K_2 is open to realize the electrical isolation between the U_1 -side and U_2 -side, which can protect the critical equipment and reduce the impact of fault.

2.2. Non-Isolated Mode

The proposed converter can also operate in the non-isolated operation mode as per a conventional converter. Similarly, there are two operating states in this mode consisting of the forward conversion stage and the reverse conversion stage. For the non-isolated mode, the trigger switch relay K_1 is switched to contact node “A”, and switch K_2 is closed during this mode, as shown in Figure 6.

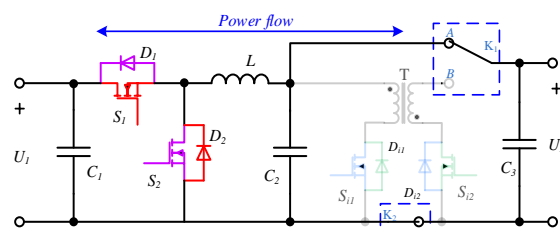


Figure 6. The equivalent circuits of the proposed converter in non-isolated operation.

The equivalent circuits for the two operation states are shown in Figure 7. In the forward conversion state, diode D_1 along with switch S_1 are used to boost the voltage, the converter transfers the power from the U_2 -side to the U_1 side, and the grid-connected power generation is a typical example of this state. Similarly, in the reverse conversion state, switch S_1 along with D_2 is used for bucking the voltage from the U_1 -side to the U_2 -side, which can draw power from the DC bus to charge the storage system.

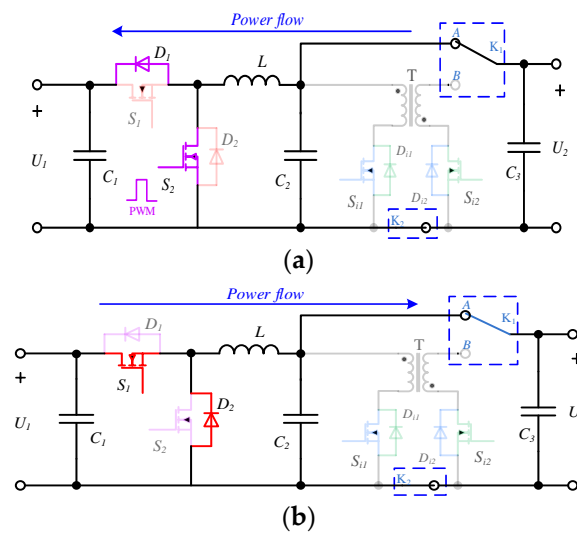


Figure 7. Two operating states of the non-isolated mode: (a) forward conversion stage; and (b) reverse conversion stage.

3. Converter Analysis and Control Strategies

The proposed original converter shown in Figure 3 is analyzed. In different operating modes, the working status of each switch is different.

3.1. Converter Analyzation during Isolated Operation Mode

According to the direction of the power flow, the isolated operation mode has two operating states: the forward conversion state and the reverse conversion state as illustrated in Figure 5a,b, respectively. It was assumed that the proposed converter operated in the continuous conduction mode (CCM), and all switches and components were ideal at the beginning. The theoretical key waveforms of the proposed converter in the isolated operation mode are shown in Figure 8.

The steady-state key conversion waveforms of the isolated mode are shown in Figure 8, where V_{gs} are the gate signals of the main switches S_1 , S_2 , S_{i1} , and S_{i2} ; K_1 and K_2 are the states of trigger switches; i_{S1} , i_{S2} and $i_{S_{i1}}$, $i_{S_{i2}}$ are the currents flowing through the main switches S_1 , S_2 , S_{i1} , and S_{i2} , respectively; i_{D1} , i_{D2} , $i_{D_{i1}}$, and $i_{D_{i2}}$ are the currents flowing through D_1 , D_2 , D_{i1} , and D_{i2} , respectively; and i_1 and i_2 are the currents flowing through U_1 -side and U_2 -side, respectively.

As presented in Figure 8a, the analyzation of the forward conversion stage in one switching period was carried out according to Figure 5a as follows: In this stage, the main switches S_1 , S_2 , and S_{i1} were turned off, and the current flows through D_{i1} and D_1 ; S_{i1} was turned on with the high frequency PWM signal where the duty ratio was adjusted. During the interval $[t_1, t_2]$, the switch S_{i2} was turned on, and the U_2 -side current path was U_2 - $K_1(B)$ - T - S_{i2} ; during the interval $[t_3, t_4]$, the switch S_{i2} was turned off, and the U_1 -side current path was T - L - D_1 - U_1 - D_{i1} . The voltage conversion ratio between the input U_2 -side and output U_1 -side is expressed as:

$$\frac{U_2}{U_1} = \frac{n_2}{n_1} \frac{D_{S_{i2}}}{1 - D_{S_{i1}}} \quad (1)$$

where n_2/n_1 is the turns ratio of the high frequency transformer; and $D_{S_{i1}}$ is the duty cycle of the PWM control signal. Based on Figures 5b and 8b, the reverse conversion stage analysis in the switching period was similar to that in the forward conversion stage. However, there was still a difference between the power flow direction and the S_1 working state. In the reverse conversion stage, the switch S_1 was OFF and the energy was transferred from the U_1 -side to U_2 -side, whose operation and voltage ratio were similar to those in the forward stage.

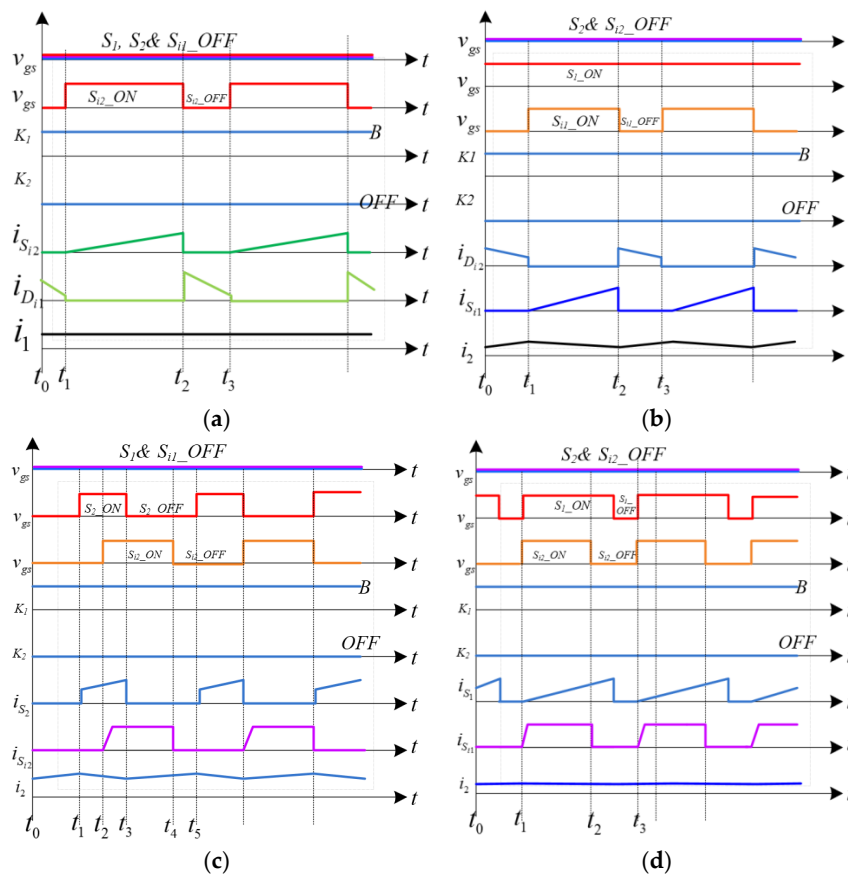


Figure 8. The key wave forms of the proposed converter in isolated mode: (a) forward mode; (b) reverse mode; (c) high-conversion-ratio step-up mode; and (d) high-conversion-ratio step-down mode.

From the above analysis, it can be seen that the output voltage can be higher or lower than the input voltage, and the duty cycle can be adjusted according to the application demands. However, if there are more high-conversion-ratio application requirements, the converter will be in a combined operation state where a high-conversion-ratio forward conversion or reverse conversion converter is obtained. In these cases, the related equivalent circuits are demonstrated in Figure 5a,b. Switches S_1 and S_2 are controlled by PWM signals, and the key waveforms for the high-conversion-ratio equivalent are also shown in Figure 5c,d, respectively.

Figure 5a shows the equivalent circuit for the high-converter-ratio forward conversion, and Figure 8c shows the control signals and key waveforms across the related components. At this stage, the converter transfers power from the U_2 -side to the U_1 -side, which is also called the forward converter stage. The switch control methods at this stage are similar to the conventional isolation forward state, except that S_2 is switched by a high frequency adjustable PWM control technique and S_1 is ON in the conventional isolation forward state. When combining the integrated control strategies, the circuit can achieve a higher and more flexible output and input ratio, which is expressed as:

$$U_1 = (k_{flyback} \cdot k_{boost}) \cdot U_2 \tag{2}$$

where $k_{flyback}$ is the equivalent isolate flyback converter ratio; and k_{boost} is the equivalent non-isolate boost converter ratio. The combination ratio is $k_{flyback} \times k_{boost}$, which can obtain a wider range of conversion ratio when compared to the conventional isolation forward state.

Similarly, Figure 5b shows the equivalent circuit of a high-converter-ratio reverse conversion, and Figure 8d shows the control pulses and key waveforms across the related components.

The analysis of the reverse conversion stage can be duplicated from the forward conversion stage. S_1 is switched by a high frequency adjustable PWM control scheme. The power transfer direction at this stage is reversed to that in the forward conversion stage when power is transferred from the U_1 -side to the U_2 -side, as is illustrated in Figure 5b. The relationship between U_1 and U_2 can be expressed as:

$$U_2 = (k_{buck} \cdot k'_{flyback}) \cdot U_1 \tag{3}$$

where k_{fbuck} is the non-isolated buck converter ratio; and $k'_{flyback}$ is the isolated flyback converter ratio. The combination ratio is $k_{buck} \times k'_{flyback}$, where a wider range of conversion ratio compared to that in the conventional isolation reverse state is derived.

According to Equations (2) and (3), it is clear that the proposed converter operating in the combination state can obtain a high conversion ratio. Therefore, compared with other types of converter topologies, the proposed converter has a wider range of applications.

3.2. Converter Analysis during Non-Isolated Operation Mode

The waveforms of the two stages under the non-isolated mode are shown in Figure 9.

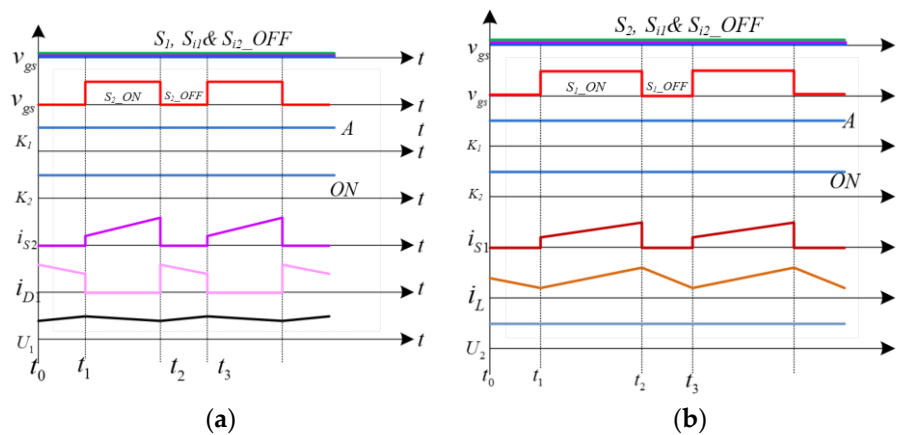


Figure 9. The key waveforms in non-isolated mode: (a) step-up mode; and (b) step-down mode.

Figure 9a shows the step-up or boost stage. According to Figure 7a, the analysis of the step-up stage is the same as that for a conventional boost converter. During the entire switching cycle, all three switches (S_1 , S_{11} , and S_{12}) are turned off. Switch S_2 is controlled by an adjustable high frequency PWM signal. The trigger switch K_1 is connected to A, and K_2 is activated. At t_1 , S_2 is turned on and i_{s1} is increased. At t_2 , S_2 is turned off and the current i_{s2} drops to zero with the power transferred to inductor L . During the step-up converter stage, the relationship between U_2 and U_1 can be expressed as:

$$U_1 = \frac{1}{1 - D_{S2}} U_2 \tag{4}$$

where D_{S2} is the duty cycle of switch S_2 .

Figure 9b shows the step-down or buck stage. According to Figure 7b, the analysis of this stage is the same as that for a conventional buck converter. Similar to the case in the forward stage, all three switches (S_2 , S_{11} , and S_{12}) are turned off during the entire switching cycle. Switch S_1 is controlled by an adjustable high frequency PWM signal. The trigger switch K_1 is connected to node A, and switch K_2 is on. At time t_1 , S_1 is turned on with i_{s1} increasing, and the energy transfers to the inductor until t_2 , when S_1 is turned off and the current i_{s1} drops to zero. During this converter stage, the relationship between U_2 and U_1 is expressed as:

$$U_1 = \frac{1}{1 - D_{S1}} U_2 \tag{5}$$

where D_{S_1} is the duty of switch S_1 .

3.3. Control Strategy

There are several different operation states or modes in the proposed new converter, so the control strategy is more complex when compared to that of a conventional single-function converter. As conventional bidirectional isolated or non-isolated converter control methods and strategies have been widely presented in the literature, details on the related control analyses and design are provided in [26–38]. Given that the proposed new converter has many different transition control strategies across different states and modes, the switching control is mainly used during the transition process between the switching devices depending on the application requirements. The state or mode transition control logic diagram is shown in Figure 10. According to our previous analysis and the illustration in Figure 10, the operation mode mainly includes the isolated and non-isolated dual modes, which are achieved by the switching control of switches K_1 and K_2 . There are many different working states in the two operation modes achieved by controlling the switches S_1 , S_2 , S_{i1} , and S_{i2} .

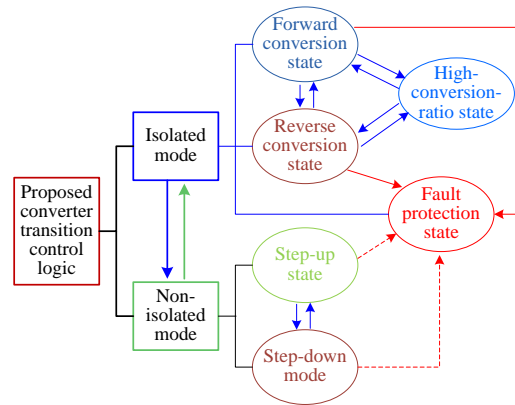


Figure 10. The transition control logic diagram of proposed converter.

According to the modes described and analyzed in Section 2, the control logics of the switches are given in Table 1. The whole control logics of the proposed converter are relatively simple as only the states of toggle switches K_1 and K_2 need to be changed when the operation mode is required to change. Furthermore, the operating stage can also be changed by controlling one or two active switches. Additionally, all switches are OFF in the fault protection mode. Thus, the control hardware implementation is relatively easy to achieve and the system cost is reduced.

Table 1. The control logics of switches states.

Switches	Control Logics						
	Isolated				Non-Isolated		
	Forward	Reverse	High-Converter-Ratio		Fault	Step-Up	Step-Down
			Forward	Reverse			
S_1	OFF	ON	OFF	PWM	OFF	OFF	PWM
S_2	OFF	OFF	PWM	OFF	OFF	PWM	OFF
S_{i1}	OFF	PWM	OFF	PWM	OFF	OFF	OFF
S_{i2}	PWM	OFF	PWM	OFF	OFF	OFF	OFF
K_1	B				A		
K_2	Disconnected				Connected		

As described above, the control flow chart for the proposed new converter is shown in Figure 11. First, the control system reads the set value and determines the operation modes and states, then according to the different operation mode or working state, it selects and calls the corresponding control method and related subroutines; then, the control signal output is calculated. Finally, the converter implements the required conversion function.

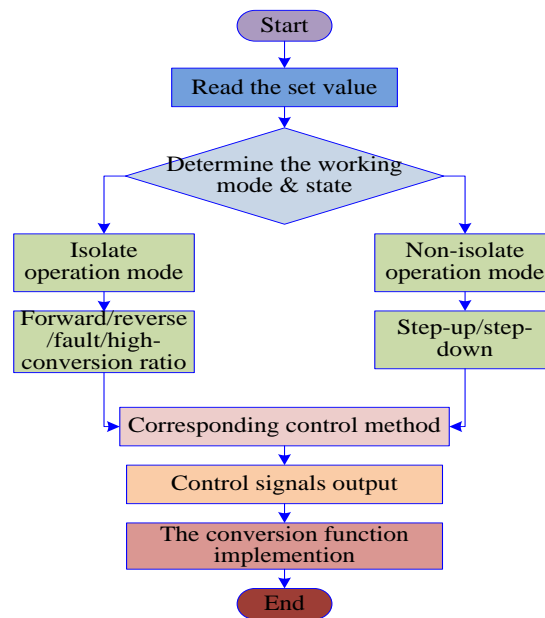


Figure 11. The control flow chart for the proposed new converter.

4. Design Consideration of Main Circuit

Based on the circuit conversion characteristics, the inductor and the transformer are the most important components of the proposed converter. Therefore, the parameter design of the non-isolated converter inductor L , and the design of the isolation converter transformer T will be discussed in this section.

4.1. Designing Non-Isolated Converter Inductor L

The non-isolated converter modes include those for the step-up and step-down conversion. Therefore, the selection of inductor L should satisfy the parameter requirements for both operation states. The design calculation and analysis of the two related modes are illustrated in [39]. The inductor L of two states can be calculated as shown in Equations (6) and (7), respectively:

$$\left\{ \begin{array}{l} I_{L(\text{step-down})} = \frac{U_{C2} \cdot (1-D_{S1}) \cdot T_{\text{step-down}}}{L_{\text{step-down}}} \\ I_{L(\text{step-down})\text{max}} = I_o - \frac{U_{C2} \cdot (1-D_{S1}) \cdot T_{\text{step-down}}}{2L_{\text{step-down}}} \\ I_{L(\text{step-down})\text{min}} = I_o - \frac{U_{C2} \cdot (1-D_{S1}) \cdot T_{\text{step-down}}}{2L_{\text{step-down}}} \\ L_{(\text{step-down})\text{min}} = \frac{U_{C2} \cdot (1-D_{(\text{step-down})}) \cdot T_{\text{step-down}}}{I_{L(\text{step-down})\text{max}}} \end{array} \right. \quad (6)$$

$$\begin{cases} I_{L(step-up)} = \frac{U_{C2} \cdot D_{S2} \cdot T_{step-up}}{L_{step-up}} \\ I_{L(step-up)max} = I_1 + \frac{U_{C2} \cdot D_{S2} \cdot T_{step-up}}{2L_{step-up}} \\ I_{L(step-up)min} = I_1 - \frac{U_{C2} \cdot D_{S2} \cdot T_{step-up}}{2L_{step-up}} \\ L_{(step-up)min} = \frac{U_{C2} \cdot D_{S2} \cdot T_{step-up}}{I_{L(step-down)max}} \end{cases} \quad (7)$$

According to Equations (6) and (7), the non-isolated converter inductor L can be selected as per Equation (8) by considering the cost and other factors, and the value can be as large as possible.

$$L = \max(L_{(step-down)min}, L_{(step-up)min}) \quad (8)$$

4.2. Designing the Isolated Converter Transformer

The design of the isolated converter transformer in the bidirectional flyback circuit is similar to that of the traditional flyback converter, which can be selected based on the experience in theoretical calculations and engineering applications. Due to the page limitations, the detailed design can be found in the related literature [40–46].

5. Simulation Test and Experimental Results

To validate the design scheme of the proposed multifunctional converter, both software simulation and experimental tests were conducted. The main parameters of the converter are summarized in Table 2.

Table 2. Main parameters of the converter.

Parameter	Value
Rated power	150 W
Capacitance $C_1/C_2/C_3$	220 μ F/220 μ F/1000 μ F
Inductance L	40 μ H
Input/output voltage range	12~100 V

5.1. Simulation Test

A Matlab/Simulink simulation model of the proposed converter was developed to validate the design scheme. The simulation experimental results from the different operation modes and working states are shown in Figures 12 and 13.

Figure 12a,b shows the key waveforms of the forward conversion under different conversion ratios. Figure 12a shows the key waveforms of the isolated flyback conventional forward operation mode, which includes the PWM control signal v_{gSi2} , the main switch S_{i2} , currents i_{Si2} and the secondary side current i_{Di2} , and the U_1 -side voltage, respectively. Figure 12b presents the key waveforms of the isolated flyback high conversion-ratio operation mode including the control signal and currents through the main switch S_{i2} currents i_{Si2} , and the inductor L current. From Figure 12, it can be seen that the proposed converter operating in the isolated mode performed well with a higher conversion ratio. The output voltage could be higher or lower than the conventional single flyback converter under the same operating condition.

The key waveforms of the non-isolated operation mode under different states are shown in Figure 13. Figure 13a presents the waveforms of the control signals, inductance current, switch and diode currents, and the output voltage in the step-up state. Figure 13b shows the waveforms of the step-down state. The control method and working waveforms are similar to those in conventional boost and buck converters.

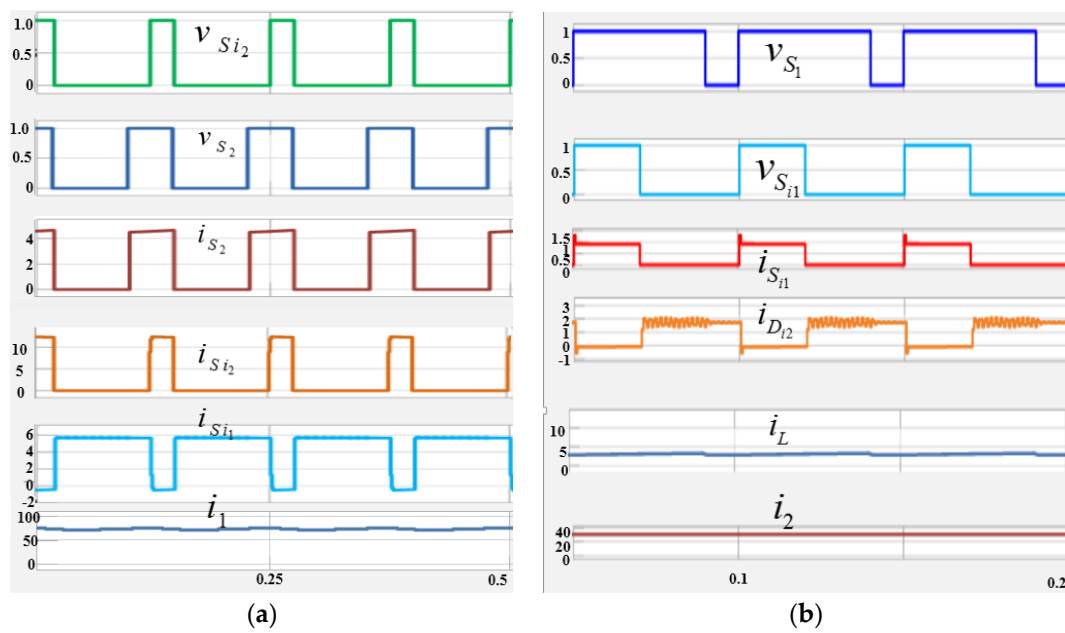


Figure 12. Simulation results for the converter under isolated mode: (a) the forward converter under isolated mode; and (b) the isolated high conversion-ratio operation mode.

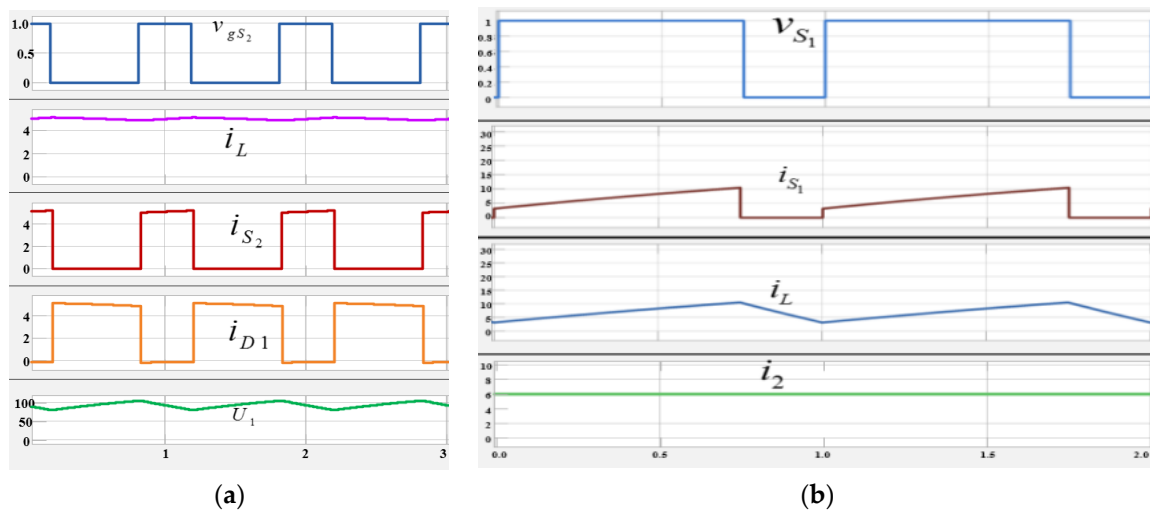


Figure 13. Simulation results for the converter under non-isolated mode: (a) the forward converter under non-isolated mode; and (b) the reserve converter under non-isolated mode.

5.2. Experimental Results

The performance and effectiveness of the proposed converter were verified in an experimental prototype. Experimental tests were conducted with a simulated photovoltaic storage application system under different operation modes and working conditions. Figure 14 shows the measured waveforms of the proposed converter in the isolated mode.

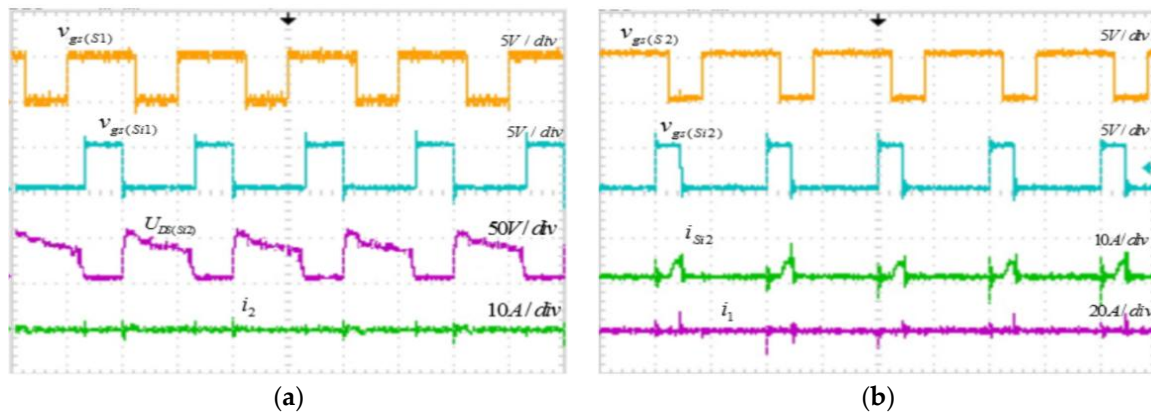


Figure 14. Experimental results for the isolated high conversion ratio operation mode: (a) step-up converter; and (b) step-down converter.

Figure 14a shows the high conversion ratio in the step-up mode. The key waveforms in the step-down converter mode are given in Figure 14b. Compared to the conventional converter, the proposed converter could simultaneously achieve isolation, and higher input and output ratios, which satisfied the requirements of the different applications.

Figure 15a shows the experimental waveforms of the non-isolated operation mode from step-up to step-down. In step-up mode, switch S_2 is controlled by the PWM signal and switch S_1 is OFF. When switching to the step-down mode, switch S_1 is controlled by the PWM signal and switch S_2 is OFF. The converter operates in the step-up/step-down state, which is similar to the operation of a conventional boost/buck converter. The proposed system can realize the transition between different operating modes by changing the switches and the control signals, and the proposed converter can be quickly changed from the isolated (reverse) mode to the non-isolated (step-up) mode as shown in Figure 15b. The experimental results showed good consistency with the theoretical analysis and simulation results.

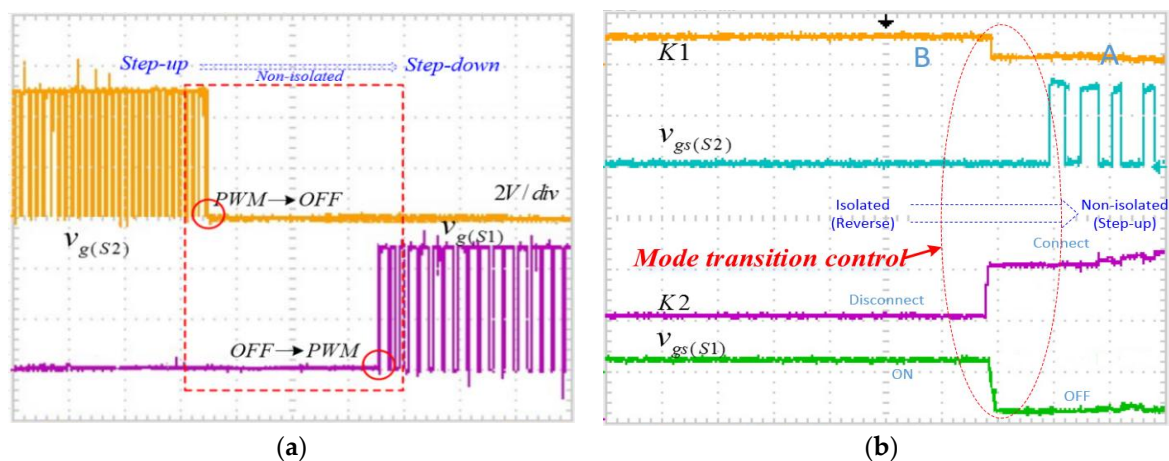


Figure 15. Experimental results for the non-isolated and mode switch: (a) step-up mode to step-down mode; and (b) mode switch.

Figure 16 depicts the efficiency curves of the proposed converter operating in different modes. As seen in the curves, the proposed converter had maximum efficiency at the non-isolated reverse mode, which was due to the single-stage power converter under high-efficiency step-down operation. The converter had relatively low efficiency at the high-conversion-ratio isolated modes due to the

reduction of the entire efficiency when the converter works in cases of high ratio, which uses two-stage circuits in series.

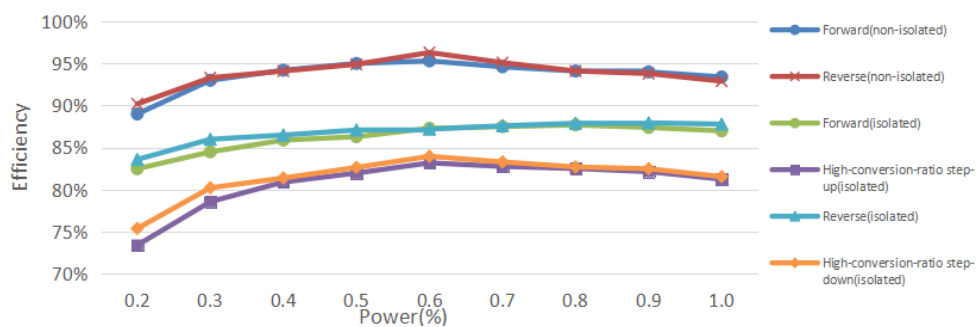


Figure 16. Efficiency curves of the proposed converter.

Table 3 presents a comparison between the proposed converter with another related bidirectional non-isolated converter studied in [47] and the isolated converter described in [48]. The proposed converter in this paper had better features including diversified operation modes, adjustable electrical isolation non-isolation, and wider voltage conversion ratios. For example, the converter mode can be changed depending on different applications. In addition, given that the relays are cheaper than switching devices, the proposed converter has almost the same cost as it has the same number of switching devices used in other related bidirectional converters.

Table 3. Comparison of the proposed converter with other bidirectional converters.

Aspect	Converter Studied in [47]	Converter Proposed in [48]	The Proposed Converter
Topology	non-isolated	Isolated	Non-isolated/isolated
Number of ports	2	3	2
Number of switches	4	4	4 + 2 *
Operating stages or modes	4	3	7
Efficiency	Higher	Higher	High **

* 2 relays; ** Specified mode.

6. Conclusions

This paper presented a multifunctional isolated and non-isolated dual-mode converter for renewable energy electrical conversion applications. The designed converter integrated the advantages of both the conventional bi-directional non-isolated converter and the isolated converter through a simple switch transition to realize multiple functions to meet different engineering application requirements. The circuit topology and composition were introduced and the working principle described in detail. Next, the different operation modes and states were analyzed. The simulation and experimental results indicated that the proposed converter could achieve dual-mode and operations under different application requirements.

Acknowledgments: This work was supported in part by a project of the Jiangsu Overseas Research and Training Program for the University, Science and Technology Project of Jiangsu Province Construction System, Science and Technology Planning Project of Suzhou City, and the Qinlan Project of Suzhou Vocational University.

Author Contributions: Yiwang Wang proposed the main idea, designed the converter, performed the experiments, and wrote the paper. Houjun Tang and Yong Yang contributed to the discussion of this research. Chun Gan, Kai Ni, and Xinhua Li double-checked and revised the whole manuscript.

Conflicts of Interest: The authors declare no conflicts of interest.

References

1. Tseng, K.; Huang, C.; Cheng, C. A Single-Switch Converter with High Step-Up Gain and Low Diode Voltage Stress Suitable for Green Power-Source Conversion. *IEEE J. Emerg. Sel. Top. Power Electron.* **2016**, *4*, 363–372. [[CrossRef](#)]
2. Xu, W.; Li, Y.; Gong, X.; Hong, Z.; Killat, D. A Dual-Mode Single-Inductor Dual-Output Switching Converter with Small Ripple. *IEEE Trans. Power Electron.* **2010**, *25*, 614–623.
3. Singh, B.; Shrivastava, A. Buck converter-based power supply design for low power light emitting diode lamp lighting. *IET Power Electron.* **2014**, *7*, 946–956. [[CrossRef](#)]
4. El Khateb, A.H.; Rahim, N.A.; Selvaraj, J.; Williams, B.W. DC-to-DC Converter with Low Input Current Ripple for Maximum Photovoltaic Power Extraction. *IEEE Trans. Ind. Electron.* **2015**, *62*, 2246–2256. [[CrossRef](#)]
5. Zeng, J.; Qiao, W.; Qu, L. An Isolated Three-Port Bidirectional DC-DC Converter for Photovoltaic Systems with Energy Storage. *IEEE Trans. Ind. Appl.* **2015**, *51*, 3493–3503. [[CrossRef](#)]
6. Kouro, S.; Leon, J.I.; Vinnikov, D.; Franquelo, L.G. Grid-Connected Photovoltaic Systems: An Overview of Recent Research and Emerging PV Converter Technology. *IEEE Ind. Electron. Mag.* **2015**, *9*, 47–61. [[CrossRef](#)]
7. Shen, C.; Shen, Y.; Tsai, C. Isolated DC-DC Converter for Bidirectional Power Flow Controlling with Soft-Switching Feature and High Step-Up/Down Voltage Conversion. *Energies* **2017**, *10*, 296. [[CrossRef](#)]
8. Tseng, S.; Wang, H. A Photovoltaic Power System Using a High Step-up Converter for DC Load Applications. *Energies* **2013**, *6*, 1068–1100. [[CrossRef](#)]
9. Xue, Y.; Chang, L.; Kjaer, S.B.; Bordonau, J.; Shimizu, T. Topologies of single-phase inverters for small distributed power generators: An overview. *IEEE Trans. Power Electron.* **2004**, *19*, 1305–1314. [[CrossRef](#)]
10. Chomsuwan, K.; Prisuwana, P.; Monyakul, V. Photovoltaic grid-connected inverter using two-switch buck-boost converter. In Proceedings of the Photovoltaic Specialists Conference, New Orleans, LA, USA, 19–24 May 2002.
11. Gonzalez, R.; Lopez, J.; Sanchis, P.; Marroyo, L. Transformerless Inverter for Single-Phase Photovoltaic Systems. *IEEE Trans. Power Electron.* **2007**, *22*, 693–697. [[CrossRef](#)]
12. Kerekes, T.; Teodorescu, R.; Rodriguez, P.; Vazquez, G.; Aldabas, E. A New High-Efficiency Single-Phase Transformerless PV Inverter Topology. *IEEE Trans. Ind. Electron.* **2011**, *58*, 184–191. [[CrossRef](#)]
13. Daher, S.; Schmid, J.; Antunes, F.L.M. Multilevel Inverter Topologies for Stand-Alone PV Systems. *IEEE Trans. Ind. Electron.* **2008**, *55*, 2703–2712. [[CrossRef](#)]
14. Sher, H.A.; Rizvi, A.A.; Addoweesh, K.E.; Al-Haddad, K. A Single Stage Stand-Alone Photovoltaic Energy System (SAPES) with High Tracking Efficiency. *IEEE Trans. Sustain. Energy* **2016**, *8*, 755–762. [[CrossRef](#)]
15. Wai, R.; Wang, W.; Lin, C. High-Performance Stand-Alone Photovoltaic Generation System. *IEEE Trans. Ind. Electron.* **2008**, *55*, 240–250. [[CrossRef](#)]
16. Wang, W.; Ruan, X. A Modified Reference of an Intermediate Bus Capacitor Voltage-Based Second-Harmonic Current Reduction Method for a Standalone Photovoltaic Power System. *IEEE Trans. Power Electron.* **2016**, *31*, 5562–5573. [[CrossRef](#)]
17. Jabir, H.; Mekhilef, S.; Nakaoka, M.; Nishida, K. Development of a transformer-based multilevel inverter topology for stand-alone photovoltaic system. In Proceedings of the Power Electronics and Applications (EPE 2013), Lille, France, 2–6 September 2013.
18. Parsekar, S.; Chatterjee, K. A Novel Strategy for Battery Placement in Standalone Solar Photovoltaic Converter System. In Proceedings of the 2014 IEEE 40th Photovoltaic Specialist Conference (PVSC), Denver, CO, USA, 8–13 June 2014; pp. 2751–2756.
19. Geibel, D.; Jahn, J.; Juchem, R. Simulation model based control development of a multifunctional PV-inverter. In Proceedings of the 2007 European Conference on Power Electronics and Applications (EPE), Aalborg, Denmark, 2–5 September 2007.
20. Wong, Y.; Chen, J.; Liu, K.; Hsieh, Y. A Novel High Step-Up DC-DC Converter with Coupled Inductor and Switched Clamp Capacitor Techniques for Photovoltaic Systems. *Energies* **2017**, *10*, 378. [[CrossRef](#)]
21. Shen, C.; Chen, H.; Chiu, P. Integrated Three-Voltage-Booster DC-DC Converter to Achieve High Voltage Gain with Leakage-Energy Recycling for PV or Fuel-Cell Power Systems. *Energies* **2015**, *8*, 9843–9859. [[CrossRef](#)]

22. Li, X.; Zhang, H.; Balog, R. Control Strategy for Seamless Transfer between Island and Grid-Connected Operation for a Dual Mode Photovoltaic Inverter. In Proceedings of the Energy Conversion Congress and Exposition (ECCE 2015), Montreal, QC, Canada, 20–24 September 2015.
23. Zeng, Z.; Yang, H.; Tang, S.; Zhao, R. Objective-Oriented Power Quality Compensation of Multifunctional Grid-Tied Inverters and Its Application in Microgrids. *IEEE Trans. Power Electron.* **2015**, *30*, 1255–1265. [[CrossRef](#)]
24. Ye, T.; Dai, N.; Lam, C.; Wong, M.; Guerrero, J.M. Analysis, Design, and Implementation of a Quasi-Proportional-Resonant Controller for a Multifunctional Capacitive-Coupling Grid-Connected Inverter. *IEEE Trans. Ind. Appl.* **2016**, *52*, 4269–4280. [[CrossRef](#)]
25. Shin, J.; Choi, S.; Cho, B. High-Efficiency Bridgeless Flyback Rectifier with Bidirectional Switch and Dual Output Windings. *IEEE Trans. Power Electron.* **2014**, *29*, 4752–4762. [[CrossRef](#)]
26. De Melo, M.F.; Vizzotto, W.D.; Quintana, P.J.; Kirsten, A.L.; Costa, M.A.D.; Garcia, J. Bidirectional Grid-Tie Flyback Converter Applied to Distributed Power Generation and Street Lighting Integrated System. *IEEE Trans. Ind. Appl.* **2015**, *51*, 4709–4718. [[CrossRef](#)]
27. Thummala, P.; Zhang, Z.; Andersen, M.A. High Voltage Bi-directional Flyback Converter for Capacitive Actuator. In Proceedings of the 2013 15th European Conference on Power Electronics and Applications (EPE), Lille, France, 2–6 September 2013.
28. Huang, X.; Lee, F.C.; Li, Q.; Du, W. High-Frequency High-Efficiency GaN-Based Interleaved CRM Bidirectional Buck/Boost Converter with Inverse Coupled Inductor. *IEEE Trans. Power Electron.* **2016**, *31*, 4343–4352. [[CrossRef](#)]
29. Viinamäki, J.; Kuperman, A.; Suntio, T. Grid-Forming-Mode Operation of Boost-Power-Stage Converter in PV-Generator-Interfacing Applications. *Energies* **2017**, *10*, 1033.
30. Zhao, F.; Zhang, X.; Wen, X.; Zhao, L.; Guo, Q.; Zhang, G. A Novel Control Scheme for Bi-directional Buck Boost Converter. In Proceedings of the 2013 International Conference on Electrical Machines and Systems, Busan, Korea, 26–29 October 2013.
31. Zhang, C.; Jiang, D.; Zheng, H.; Ye, L. A Bi-directional Buck/Boost Voltage Balancer for DC Distribution System. In Proceedings of the Fourth International Conference on Digital Manufacturing & Automation, Qindao, China, 29–30 June 2013.
32. Ardi, H.; Ahrabi, R.R.; Ravadanegh, S.N. Non-isolated bidirectional DC-DC converter analysis and implementation. *IET Power Electron.* **2014**, *7*, 3033–3044. [[CrossRef](#)]
33. Zheng, X.; Ali, H.; Wu, X.; Zaman, H.; Khan, S. Non-Linear Behavioral Modeling for DC-DC Converters and Dynamic Analysis of Distributed Energy Systems. *Energies* **2017**, *10*, 63. [[CrossRef](#)]
34. Hamasaki, S.; Yano, Y.; Fukuda, H.; Tsuji, M. Deadbeat Control of Bidirectional Buck/boost DC-DC Converter for Power Leveling System with EDLC. In Proceedings of the 2015 41st IEEE Annual Conference of the Industrial Electronics Society, Yokohama, Japan, 9–12 November 2015.
35. McCurlie, L.; Preindl, M.; Malysz, P.; Emad, A. Simplified Control for Redistributive Balancing Systems using Bidirectional Flyback Converters. In Proceedings of the 2015 IEEE Transportation Electrification Conference and Expo (ITEC2015), Dearborn, MI, USA, 14–17 June 2015.
36. Hoffstadt, T.; Maas, J. Sensorless BCM control for a bidirectional flyback-converter. In Proceedings of the 42nd Annual Conference of the IEEE Industrial Electronics Society, IECON 2016, Florence, Italy, 24–27 October 2016.
37. Thummala, P.; Maksimovic, D.; Zhang, Z.; Andersen, M.A.E. Digital Control of a High-Voltage (2.5 kV) Bidirectional DC-DC Flyback Converter for Driving a Capacitive Incremental Actuator. *IEEE Trans. Power Electron.* **2016**, *31*, 8500–8516. [[CrossRef](#)]
38. Saranya, P.S.; Chandran, L.R. Analysis of bidirectional flyback converter. In Proceedings of the 2015 International Conference on Computation of Power, Energy, Information and Communication (ICCPEIC), Chennai, India, 22–23 April 2015.
39. Pressman, A.I.; Billings, K.H.; Morey, T. *Switching Power Supply Design*, 3rd ed.; McGraw-Hill: New York, NY, USA, 2009.
40. Trzynadlowski, A.M. *Power Electronic Converters and Systems: Frontiers and Applications*; The Institution of Engineering and Technology: London, UK, 1 February 2016.
41. Patin, N. *Power Electronics Applied to Industrial Systems and Transports*; ISTE Press and Elsevier: London, UK, May 2015; Chapter 2; pp. 19–39.

42. Padiyar, U.S.; Kamath, V. Design and Implementation of a Universal Input Flyback Converter. In Proceedings of the International Conference on Electrical, Electronics, and Optimization Techniques (ICEEOT), Chennai, India, 3–5 March 2016; pp. 3428–3433.
43. Lee, I.; Lee, J. A High-Power DC-DC Converter Topology for Battery Charging Applications. *Energies* **2017**, *10*, 871. [[CrossRef](#)]
44. Hu, J.; Cheng, K.W.E. Predictive control of power electronics converters in renewable energy systems. *Energies* **2017**, *10*, 515. [[CrossRef](#)]
45. Chung, H.S.H.; Cheung, W.; Tang, K. A ZCS Bidirectional Flyback Converter. In Proceedings of the 2004 35th Annual IEEE Power Electronics Specialists Conference, Aachen, Germany, 20–25 June 2004; pp. 1506–1512.
46. Wu, H.; Sun, K.; Chen, L.; Zhu, L.; Xing, Y. High Step-Up/Step-Down Soft-Switching Bidirectional DC-DC Converter with Coupled-Inductor and Voltage Matching Control for Energy Storage Systems. *IEEE Trans. Ind. Electron.* **2016**, *63*, 2892–2903. [[CrossRef](#)]
47. Liu, K.; Liu, C.; Liu, Y.; Chien, Y.; Wang, B. Analysis and Controller Design of a Universal Bidirectional DC-DC Converter. *Energies* **2016**, *9*, 501. [[CrossRef](#)]
48. Wu, Y.; Chiu, P. A High-Efficiency Isolated-Type Three-Port Bidirectional DC/DC Converter for Photovoltaic Systems. *Energies* **2017**, *10*, 434. [[CrossRef](#)]



© 2017 by the authors. Licensee MDPI, Basel, Switzerland. This article is an open access article distributed under the terms and conditions of the Creative Commons Attribution (CC BY) license (<http://creativecommons.org/licenses/by/4.0/>).